American Mineralogist, Volume 96, pages 864–868, 2011

Density measurement of liquid FeS at high pressures using synchrotron X-ray absorption

Keisuke Nishida,[1,*] Eiji Ohtani,[1] Satoru Urakawa,[2] Akio Suzuki,[1] Tatsuya Sakamaki,[1] Hidenori Terasaki,[1] and Yoshinori Katayama[3]

[1]Department of Earth and Planetary Materials Science, Tohoku University, Sendai 980-8578, Japan
[2]Department of Earth Science, Okayama University, Okayama 700-8530, Japan
[3]Japan Atomic Energy Agency, Hyogo 679-5143, Japan

Abstract

The density of liquid iron sulfide (FeS) was measured up to 3.8 GPa and 1800 K using an X-ray absorption method. The compression curve of liquid FeS was fitted using the Vinet equation of state. The isothermal bulk modulus and its temperature and pressure derivatives were determined using a nonlinear least-squares fit. The parameter sets determined were: K_{0T} = 2.5 ± 0.3 GPa at T = 1500 K, $(dK_0/dT)_P$ = –0.0036 ± 0.0003 GPa/K, and $(dK_0/dP)_T$ = 24 ± 2. These results suggest that liquid FeS is more compressible than Fe-rich liquid Fe-S.

Keywords: X-ray absorption method, liquid FeS, density, high pressure, equation of state

Introduction

The Earth's outer core is thought to be composed of iron alloys with a small amount (8–11 wt%) of light elements, such as sulfur (e.g., Birch 1952). The geodynamo in the Earth's liquid outer core generates its intrinsic magnetic field. Magnetic fields have also been observed in the planet Mercury by the Mariner 10 probe (Ness et al. 1975) and in Jupiter's moon, Ganymede, by the Galileo spacecraft (Kivelson et al. 1996). These observations suggest that both Mercury and Ganymede have liquid cores (e.g., Stevenson 1987; Schubert et al. 1996; Sarson et al. 1997). Moreover, quasi-parallel bands of magnetized crust with alternating polarity have been recorded by the Mars Global Surveyor spacecraft, which strongly suggests the existence of an ancient magnetic field on Mars (Acuña et al. 1999; Connerney et al. 2005; Solomon et al. 2005). The internal temperature of these smaller bodies is likely to be lower than that of the Earth (e.g., Breuer et al. 2007; Kimura et al. 2009), and since sulfur reduces the melting point of metallic iron (e.g., Brett and Bell 1969), the molten cores of these planets and satellites may be composed of liquid Fe-S alloys. Thus, the physical properties of liquid Fe-S alloys are important in gaining an understanding of the core dynamics of these planets and satellites.

Knowledge of the density of liquid Fe-S is a fundamental parameter for the study of the internal structure and dynamics of the cores of these bodies. Recently, the sink/float and X-ray absorption methods have been used to measure the density of metallic liquids under static high-pressure conditions. Balog et al. (2001, 2003) carried out measurements on liquid Fe-10wt%S up to 20 GPa using the sink/float method and obtained a bulk modulus of K_{0T} = 63 GPa. Nishida et al. (2008) measured the density of liquid Fe-S at 4 GPa, and showed the influence of the sulfur content on the density of this system. Previously, Sanloup et al. (2000) had measured the density of Fe-S (for S = 10, 20, and 27 wt%) at 1.5–6.2 GPa and 1500–1780 K using an X-ray absorption method, which had been developed by Katayama et al. (1993) and Katayama (1996), and showed the effect of the sulfur content on the isothermal bulk modulus (K_T) of liquid Fe-S. Chen et al. (2005) measured the density of liquid FeS at 4.1 GPa and 1573 K using an X-ray absorption method employing radiographic images. However, the effect of pressure on the density, i.e., the bulk modulus K_T and its pressure derivative $(dK_0/dP)_T$, of liquid FeS has not been reported to date. In this study, we measured the density of liquid FeS up to 3.8 GPa and 1800 K using an X-ray absorption technique and determined the equation of state (EOS) of liquid FeS.

Experimental methods

High-pressure experiments were performed using a DIA-type cubic anvil press (SMAP-I) installed at the in-vacuum undulator beamline BL22XU at the SPring-8 facility in Japan (Sakamaki et al. 2009, 2010). The synchrotron X-rays were monochromatized using a double-Si (111) crystal monochromator with the X-ray energy tuned to 30 keV. The size of the incident X-ray was reduced to 50 × 50 μm using two pairs of slits. The intensity of the incident X-rays (I_0) and transmitted X-rays (I) was measured simultaneously using two ion chambers. The X-ray diffraction pattern was also recorded using an imaging plate detector.

We used the high-pressure cell assembly described by Sakamaki et al. (2009, 2010), except for sample capsule. In this study, a cylindrical single-crystal sapphire with boron nitride (BN) lids was used as the sample container. The sapphire capsule was assumed to be compressed uniformly within the experimental conditions used because of its high bulk modulus. The sample geometry is shown in Figure 1a. The outer and inner diameters of the sapphire cylinder were 1.0 and 0.5 mm, respectively, and its height was 1.0 mm. The sample was easily compressed by displacement of the BN lids under compression. The starting material was FeS powder (Rare Metallic Co. Ltd., 99.9% in purity). We performed chemical analysis on the recovered samples using SEM/EDS and confirmed that the FeS was not contaminated by any surrounding material, such as Al_2O_3 or BN. The composition of the recovered samples was $Fe_{48.7}S_{51.3}$. The pressure was calculated using the EOS of MgO (Jamieson et al. 1982) and BN (Urakawa et al. 1993) pressure markers. The temperature of the sample was monitored using a $W_{97}Re_3$-$W_{75}Re_{25}$ thermocouple.

We measured the X-ray absorption profile (I/I_0) along the radial direction of the cylindrical sample by moving the press stage in 10 μm intervals (Fig.

* E-mail: nishidak@m.tains.tohoku.ac.jp

0003-004X/11/0506–864$05.00/DOI: 10.2138/am.2011.3616

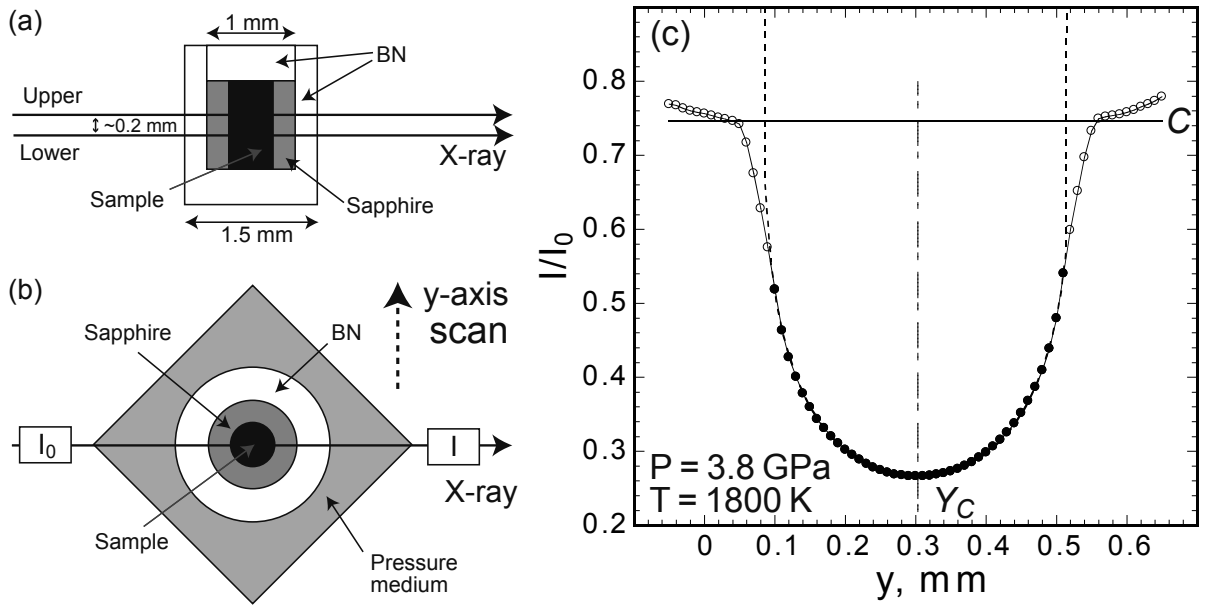

FIGURE 1. (**a**) A cross-section of the center of the cell assembly. The upper and lower sections denote the sample position relative to its height in the press, i.e., the **z**-axis of the press, where the absorption profile of the sample was measured. (**b**) A schematic view of the scan geometry. (**c**) A typical X-ray transmission profile of liquid FeS at 1800 K and 3.8 GPa. The open and solid circles denote the observed I/I_0 values. The dashed curve is the regression curve fit (solid circles) to Equation 5. The vertical dashed-dotted line denotes the center of the capsule, Y_c. The solid line represents parameter C in Equation 5, determined from the inflection points in I/I_0 corresponding to the boundary between the sample and the sapphire ring.

1b). It took about 5 min to obtain a single X-ray absorption profile across the sample; an example of an obtained absorption profile is shown in Figure 1c. After obtaining absorption profiles, we collected the X-ray diffraction spectra of the sample and the pressure markers. These measurements were carried out while increasing the temperature under a fixed load. We evaluated the density of liquid FeS from the X-ray absorption profiles after carrying out the data reduction procedure outlined below.

The X-ray absorption method is based on the Beer–Lambert law:

$$\frac{I}{I_0} = \exp\left[\left(-\mu\rho t\right)_{\text{Sample}} + \left(\mu\rho t\right)_{\text{Sapphire}} + \left(-\mu\rho t\right)_{\text{environment}}\right] \quad (1)$$

where I_0 and I are the intensities of the incident and transmitted X-ray, μ is the X-ray mass absorption coefficient, ρ is the density, and t is the thickness. Assuming that the absorption of the surrounding materials, such as the pressure medium and heater surrounding the sapphire capsule, was uniform across the sample, we obtain

$$\frac{I}{I_0}(y) = C\exp\left[\left(-\mu\rho t\right)_{\text{Sample}} + \left(-\mu\rho\Delta t\right)_{\text{Sapphire}}\right] \quad (2)$$

$$t = 2\sqrt{r^2 - \left(y - Y_c\right)^2} \quad (3)$$

$$\Delta t = \left(2\sqrt{R^2 - \left(y - Y_c\right)^2} - 2\sqrt{r^2 - \left(y - Y_c\right)^2}\right) - 2\sqrt{R^2 - r^2} \quad (4)$$

where y is the displacement in the direction perpendicular to the X-ray beams, R and r are the outer and inner radii of the sapphire capsule, respectively, and Y_c is the y coordinate of the sample center. The parameter C is the X-ray absorption at the boundary between the sapphire and the sample, and the value of C can be evaluated graphically (see Fig. 1c). The path length of the X-rays traveling through the sapphire ring changes with y. The second term in the exponential function on the right-hand side of Equation 2 is a correction term for the difference in contribution from the term Δt from the sapphire capsule from the X-ray path to X-ray absorption, which is 0 mm at $y = Y_C \pm r$ and approx. –0.366 mm at $y = Y_C$. Substituting Equations 3 and 4 into Equation 2, we obtain $f(y)$

$$f(y) = \frac{I}{I_0}(y) = C\exp\left[\left\{-2\mu\rho\sqrt{r^2 - \left(y - Y_c\right)^2}\right\}_{\text{Sample}}\right. \quad (5)$$

$$\left. + \left\{-2\mu\rho\left(\left(\sqrt{4r^2 - \left(y - Y_c\right)^2} - \sqrt{r^2 - \left(y - Y_c\right)^2}\right) - \sqrt{3r^2}\right)\right\}_{\text{Sapphire}}\right]$$

where the outer radius of the sapphire capsule is assumed to be $R = 2r$. The inner radius of the sapphire capsule, r, also changes elastically with pressure and temperature, and its value, as well as the density, can be evaluated using a least-squares fit. The X-ray mass absorption coefficient and the density of the sapphire were evaluated using a theoretical formula (Chantler 1995) and the EOS for Al_2O_3 (Pavese 2002), respectively. The mass absorption coefficient of the sample (μ_{Sample}) is then the unknown parameter for determining the sample density and radius.

Katayama (1996) reported that the density obtained using the X-ray absorption method (the absorption density) systematically shifts away from the actual density because of an uncertainty in the theoretical mass absorption coefficient. Therefore, the mass absorption coefficient of the sample was calibrated using the incident monochromatic X-rays in each experiment. We determined the X-ray mass absorption coefficient, μ, of the sample experimentally by substituting the density of crystalline FeS obtained from X-ray diffraction measurements into Equation 5, combined with the X-ray absorption profile. These measurements were carried out at 900 K under pressure, where the pore spaces between the powder sample were compacted and the deviatoric stress in the sample was relaxed. We determined the X-ray mass absorption coefficient at different sample positions (the upper and lower positions shown in Fig. 1b) to improve the reliability of the obtained density values.

We evaluated the error propagated from the counting error of I and I_0 (0.5%), the uncertainty of μ_{FeS} (~1%), the fitting error (~1.5%), and the standard deviation from multiple measurements at different sample positions (~1.5%). The estimated error in the measured density was <2%.

Results and discussion

Figure 1c shows a typical X-ray transmission profile of liquid FeS at 3.8 GPa and 1800 K, which shows the high contrast between the sapphire capsule and the sample. The data points used for the profile fitting to Equation 5 were at the center of the parabolic section, except for four points near the inflection points on both sides, corresponding to the sample-capsule boundaries. This pattern occurred because these points were located within the slit size of 50 μm, where the absorption was influenced by the sapphire capsule.

The X-ray mass absorption coefficient and value of the density of liquid FeS in each experimental run are listed in Table 1. The measured X-ray mass absorption coefficients, except for Run B165, are consistent with the theoretical value of pure FeS at 30 keV, which ranges from 5.5 to 6.0 cm^2/g (Hubbell 1982; Seltzer 1993; Henke et al. 1993; Chantler 1995). However, the measured X-ray mass absorption coefficients varied slightly at different sample positions (i.e., the lower and upper positions in Table 1), as well as between different experimental runs. The reason for this discrepancy is unclear, but it can be attributed partly to the uncertainty in the parameter *C* in Equation 2, which was evaluated graphically, and from small irregularities in the absorption profiles because of the heterogeneity of the surrounding materials (e.g., the pressure medium and the heater), which were assumed to be uniform. These factors gave rise to the estimation error in the mass absorption coefficient, and also to an additional error in the density values through the fitting process of each profile. However, a comparison of the absorption density at different sample positions showed that the effect of these factors on the density was minor.

Figure 2 shows that the absorption density at the upper and lower positions was consistent across all the temperature ranges studied, regardless of whether the sample was solid or liquid, when the absorption density was calculated using the X-ray mass absorption coefficients determined at 900 K for each sample position. The parameter *C* was estimated graphically using the intensity of the X-rays passing through the incident slit with a finite size. If the sample position varied with temperature, then parameter *C* would change in each absorption profile acquired at a different temperature. However, the spatial configuration of the sample cell assembly was effectively constant during the heating cycle of each run. Therefore, the graphical method provided a good estimation of parameter *C* at a fixed sample position, and the sample environmental conditions were also kept constant at each sample position during heating. The similarity in the change in density with temperature at different sample positions provides assurance that the X-ray absorption measurements provide a reasonable relative precision of the measured density.

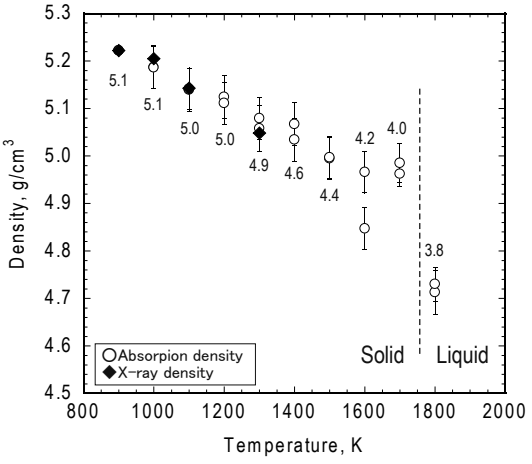

Figure 2. Density of FeS as a function of temperature under a constant load of 100 tons. The solid diamonds denote the density of solid FeS V (NiAS-type) determined from X-ray diffraction data. The open circles denote the density of FeS obtained using the X-ray absorption method. The numerals denote the pressure (in GPa). The vertical dashed line denotes the melting temperature estimated from the discontinuous change in density.

Figure 2 also shows that the density determined from X-ray diffraction data (the diffraction density) agrees with the absorption density in the temperature range 1000–1300 K within the experimental error. The thermal expansion coefficient, α, of solid FeS was also derived from the X-ray absorption data, showing $\alpha = 1.0 \times 10^{-4}$ K^{-1} around 0.8 GPa, and $\alpha = 6.9 \times 10^{-5}$ K^{-1} around 4.5 GPa. These values are consistent with the values reported by Kusaba et al. (2000) and Urakawa et al. (2004). These results confirm that the X-ray absorption method provides a reliable density value with a reasonable accuracy.

From Figure 2, it can be seen that a sharp decrease in the density (about 5%) occurred between 1700 and 1800 K during heating under a constant load of 100 tons, even though the pressure decreased with increasing temperature. This large change in density can only be accounted for by the melting of the sample. We determined the melting temperatures of FeS based on this criterion, and this was consistent with values determined in previous melting experiments (Sharp 1969; Ryzhenko and Kennedy

Table 1. Experimental conditions and results

Run no.	Pressure (GPa)	Temperature (K)	Lower position*		Upper position*	
			X-ray mass absorption coefficient (cm^2/g)	Density (g/cm^3)	X-ray mass absorption coefficient (cm^2/g)	Density (g/cm^3)
B165	0.4 ± 0.1	1500†	5.36 ± 0.06	Solid	5.21 ± 0.04	4.38 ± 0.06
	0.4 ± 0.1	1600†		4.23 ± 0.05		4.32 ± 0.06
B139	2.2 ± 0.1	1600	5.86 ± 0.05	4.58 ± 0.06	5.75 ± 0.05	4.61 ± 0.06
	2.1 ± 0.1	1700		4.55 ± 0.06		4.55 ± 0.06
B155	2.8 ± 0.1	1700†	5.66 ± 0.08	4.62 ± 0.04	5.75 ± 0.08	4.64 ± 0.05
	2.6 ± 0.1	1800†		4.59 ± 0.04		4.61 ± 0.06
B154	3.8 ± 0.1	1800	5.52 ± 0.05	4.71 ± 0.05	5.47 ± 0.05	4.73 ± 0.04

* Upper and lower positions denote the sample position relative to its height in the press, i.e., the **z**-axis of the press, where the absorption profile of the sample was measured (Fig. 1a).
† Temperature was estimated by power-temperature relation.

1973). However, we could not identify any melting of the sample from the X-ray diffraction pattern, because the diffraction pattern was spotty due to grain growth of solid FeS near the melting temperature. It was difficult to detect the diffraction spots using an imaging plate, because the detection area was limited by the narrow gap between the tungsten carbide anvils at high pressure.

Figure 3 shows the effect of pressure on the density of liquid FeS. Our density value of liquid FeS at 1800 K and ~4 GPa was close to the value determined by Chen et al. (2005) at 4.2 GPa and 1573 K. However, the experimental conditions of Chen et al. (2005) were clearly lower than those for the reported melting curve of FeS (Sharp 1969; Ryzhenko and Kennedy 1973). However, because Chen et al. (2005) placed their thermocouple outside the tube heater, they may have underestimated the sample temperature, and if their measured temperature was really around 1800 K, just above melting point, then their density is consistent with our data.

The density of liquid $Fe_{48.7}S_{51.3}$ at 1500 K and atmospheric pressure was calculated to be 3.67 g/cm^3 from maximum bubble data (Nagamori 1969). Adopting this zero-pressure density, the density of liquid FeS increases sharply between 0 and 0.5 GPa. The density change due to melting, which is calculated by the extrapolated density of solid FeS V (NiAs-type) (Selivanov et al. 2003; Tenailleau et al. 2005) and liquid FeS (Nagamori 1969; Kaiura and Toguri 1979), is about 15% at ambient pressure and larger than 5% at 3.8 GPa. The sharp increase in density of liquid FeS suggests the existence of a structural change in the liquid below 0.5 GPa. Urakawa et al. (1998) reported that there was no significant difference in the structure of liquid FeS between 1.5 and 5.3 GPa, whereas the structure of liquid FeS has not been reported at ambient pressure.

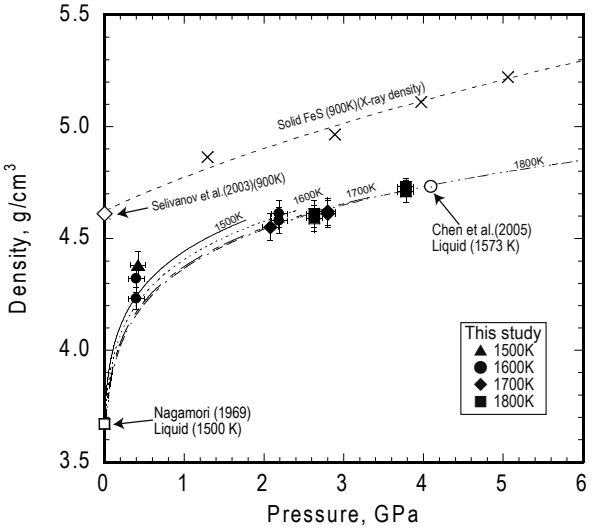

FIGURE 3. Density as a function of pressure. The solid symbols denote the density of liquid FeS obtained using the X-ray absorption method in this study. The open circles denote the density of liquid FeS at 1573 K determined by Chen et al. (2005). The open squares denote the density of liquid FeS at 1500 K and ambient pressure estimated by Kaiura and Toguri (1979). The solid, dotted, dashed-dotted, and dashed-dotted-dotted curves denote the compression of liquid FeS at 1500, 1600, 1700, and 1800 K, respectively, fitted using the Vinet equation of state. The crosses denote the density of solid FeS V at 900 K determined using X-ray diffraction. The open diamonds denote the density of solid FeS V at 900 K and 1 atm (Selivanov et al. 2003).

We fitted the pressure-density-temperature data using the Vinet EOS, which is superior to other types of EOS for soft materials, such as liquids (Vinet et al. 1989). The Vinet EOS is given by the following expression

$$P(\rho,T) = 3K_{0T}(T)\left(\frac{\rho_0(T)}{\rho(T)}\right)^{-\frac{2}{3}}\left[1-\left(\frac{\rho_0(T)}{\rho(T)}\right)^{\frac{1}{3}}\right] \exp\left\{\frac{3}{2}\left[\left(\frac{\partial K_0}{\partial P}\right)_T - 1\right]\left[1-\left(\frac{\rho_0(T)}{\rho(T)}\right)^{\frac{1}{3}}\right]\right\} \quad (6)$$

$$K_{0T}(T) = K_{0T}(T_0) + \left(\frac{\partial K_0}{\partial T}\right)_P (T - T_0) \quad (7)$$

$$\rho_0(T) = \frac{\rho_0(T_0)}{\exp\left(\int_{T_0}^{T} \alpha dT\right)} \quad (8)$$

where ρ_0 is the density at atmospheric pressure. The isothermal bulk modulus at atmospheric pressure is denoted by K_{0T}, T, and T_0 are the temperature of the sample and the reference temperature, respectively, and α is the thermal expansion coefficient. Because we measured the density of liquid FeS between 1500 and 1800 K, the value of T_0 was set to T_0 = 1500 K. Thus, the bulk modulus $K_{0,1500\,K}$, its temperature derivative $(dK_0/dT)_P$, and the pressure derivative $(dK_0/dP)_T$ were determined simultaneously by fitting all the density data to Equations 6, 7, and 8 using a nonlinear least-squares method, where α was fixed to the reported value of $\alpha = 1.6 \times 10^{-3}$ K^{-1} (Kaiura and Toguri 1979). The derived parameters to fit the data were: $K_{0,1500\,K} = 0.4 \pm 0.2$ GPa, $(dK_0/dT)_P = -0.0005 \pm 0.0001$ GPa/K, and $(dK_0/dP)_T = 29 \pm 4$ (Table 2). The estimated value of $(dK_0/dT)_P$ was much lower than that of liquid iron (–0.024 GPa/K) (Hixson et al. 1990) and that of solid FeS V (–0.0117 ± 0.0015 GPa/K) (Urakawa et al. 2004). More detailed work is required to improve the accuracy of K_{0T} and $(dK/dT)_P$. Sanloup et al. (2000) reported that the value of K_T in the Fe-FeS system decreases with increasing sulfur content from 82.5 GPa for S = 0% to 12.9 GPa for S = 39.2 at%. Our value of K_{0T} is consistent with the extrapolated value from Sanloup et al.'s data. Although Sanloup et al. (2000) determined their bulk modulus using the Birch-Murnaghan EOS with $(dK_0/dP)_T$ = 4–7, we could not fit our density smoothly except when using the Vinet EOS with a large value of $(dK_0/dP)_T = 29 \pm 4$.

TABLE 2. Parameters of equation of state for liquid FeS

	Liquid FeS	
Pressure (GPa)	All	0.5<
T_0 (K)	1500	1500
$K_{0,1500\,K}$ (GPa)	2.5 ± 0.3	12 ± 3
dK_0/dP	24 ± 2	14 ± 3
dK_0/dT (GPa/K)	–0.0036 ± 0.0003	–0.016 ± 0.003
$\rho^0_{0,1500\,K}$ (g/cm^3)	3.67*	4.23 ± 0.03
a (×10^{-4} K^{-1})†	1.6 ± 0.3	1.6 ± 0.3

* Calcurated form Nagamori (1969).
† Calcurated form Kaiura and Toguri (1979).

This may be explained by an increase in the density associated with a possible structural change in liquid FeS at pressures <0.5 GPa. If we use the liquid density values for pressures above 0.5 GPa, where no structural change in liquid FeS was observed by Urakawa et al. (1998), then we obtain $K_{1500\,K} = 12 \pm 3$ GPa, with $(dK_0/dP)_T = 14 \pm 3$ and $(dK/dT)_P = -0.016 \pm 0.003$. Therefore, this value of K_T is also smaller than that of an Fe-rich Fe-S melt. Liquid FeS is more compressible than an Fe-rich Fe-S liquid. However, our results are based on a limited number of data points, and so further experimental studies under a wider pressure range, especially below 0.5 GPa, are required to clarify the details of the rapid increase in density in the compression curve around 0.5 GPa, and to improve the accuracy of the values of K_{0T} and $(dK/dT)_P$.

Acknowledgments

This work was supported by a Grant-in-Aid for scientific research to E.O. (no. 18104009 and 22000002) and S.U. (13440163 and 16340170) from the Ministry of Education, Culture, Sports, Science, and Technology of the Japanese Government. This work was also partially supported by the Global Center-of-Excellence Program, "Global Education and Research Center for Earth and Planetary Dynamics." K.N. was supported by a Research Fellowship of the Japan Society for the Promotion of Science for Young Scientists. The synchrotron radiation experiments were performed at the BL22XU line of the JAEA SPring-8 facility under the Common-Use Facility Program of JAEA (Proposal No. 2006A-E17, 2007A-E31, and 2007B-E12).

References cited

Acuña, M.H., Connerney, J.E.P., Ness, N.F., Lin, R.P., Mitchell, D., Carlson, C.W., McFadden, J., Anderson, K.A., Rème, H., Mazelle, C., Vignes, D., Wasilewski, P., and Cloutier, P. (1999) Global distribution of crustal magnetization discovered by the Mars Global Surveyor MAG/ER experiment. Science, 284, 790–793.

Balog, P.S., Secco, R.A., and Rubie, D.C. (2001) Density measurements of liquids at high pressure: Modification to the sink/float method by using composite spheres, and application to Fe-10wt%S. High Pressure Research, 21, 237–261.

Balog, P.S., Secco, R.A., Rubie, D.C., and Frost, D.J. (2003) Equation of state of liquid Fe-10 wt % S: Implications for the metallic cores of planetary bodies. Journal of Geophysical Research, 108, 2124, DOI: 10.1029/2001JB001646.

Birch, F. (1952) Elasticity and constitution of the Earth's interior. Journal of Geophysical Research, 57, 227–286.

Brett, R. and Bell, P.M. (1969) Melting relations in the Fe-rich portion of the system Fe–FeS at 30 kb pressure. Earth and Planetary Science Letters, 6, 479–482.

Breuer, D., Hauck, S.A. Buske, M., Pauer, M., and Spohn, T. (2007) Interior evolution of Mercury. Space Science Reviews, 132, 229–260, DOI: 10.10007/s11214-007-9228-9.

Chantler, C.T. (1995) Theoretical form factor, attenuation and scattering tabulation for Z = 1–92 from E = 1–10 eV to E = 0.4–1.0 MeV. Journal of Physical and Chemical Reference Data, 24, 71–643.

Chen, J., Weidner, D.J., Wang, L., Vaughan, M.T., and Young, C.E. (2005) Density measurements of molten materials at high pressure using synchrotron X-ray radiography: Melting volume of FeS. In J. Chen, Y. Wang, T.S. Duffy, G. Shen, L.F. Dobrzhinetskaya, Eds., Advances in high-pressure technology for geophysical applications, p. 185–194. Elsevier, Amsterdam.

Connerney, J.E.P., Acuña, M.H., Ness, N.F., Kletetschka, G., Mitchell, D.L., Lin, R.P., and Rème, H. (2005) Tectonic implications of Mars crustal magnetism. Proceedings of the National Academy of Sciences, 102, 14970–14975.

Henke, B.L., Gullikson, E.M., and Davis, J.C. (1993) X-ray interactions: Photoabsorption, scattering, transmission, and reflection at $E = 50–30{,}000$ *eV, Z* = 1–92. Atomic Data and Nuclear Data Tables, 54, 181–342.

Hixson, R.S., Winkler, M.A., and Hodgdon, M.L. (1990) Sound speed and thermophysical properties of liquid iron and nickel. Physical Review B, 42, 6485–6491.

Hubbell, J.H. (1982) Photon mass attenuation and energy-absorption coefficients from 1 keV to 20 MeV. The International Journal of Applied Radiation and Isotopes, 33, 1269–1290.

Jamieson, J.C., Fritz, J.N., and Manghnani, M.H. (1982) Pressure measurement at high temperature in X-ray diffraction studies: Gold as a primary standard. In S. Akimoto, M.H. Manghnani, Eds., High-Pressure Research in Geophysics, p. 27–48. Center for Academic Publications, Tokyo.

Kaiura, G.H. and Toguri, J.M. (1979) Densities of the molten FeS, FeS–Cu_2S and Fe–S–O systems—utilizing a bottom-balance Archimedean technique. Canadian Metallurgical Quarterly, 18, 155–164.

Katayama, Y. (1996) Density measurements of non-crystalline materials under high pressure and high temperature. High Press Research, 14, 383–391.

Katayama, Y., Tsuji, K., Chen, J.-Q., Koyama, N., Kikegawa, T., Yaoita, K., and Shimomura, O. (1993) Density of liquid tellurium under high pressure. Journal of Non-Crystalline Solids, 156–158, 687–690.

Kimura, J., Nakagawa, T., and Kurita, K. (2009) Size and compositional constraints of Ganymede's metallic core for driving an active dynamo. Icarus, 202, 216–224.

Kivelson, M.G., Khurana, K.K., Russell, C.T., Walker, R.J., Warnecke, J., Coroniti, F.V., Polanskey, C., Southwood, D.J., and Schubert, G. (1996) Discovery of Ganymede's magnetic field by the Galileo spacecraft. Nature, 384, 537–541.

Kusaba, K., Utsumi, W., Yamanaka, M., Shimomura, O., and Syono, Y. (2000) Second-order phase transition of FeS under high pressure and temperature. Journal of Physics and Chemistry of Solids, 61, 1483–1487.

Nagamori, M. (1969) Density of molten Ag-S, Cu-S, and Ni-S systems. Transactions of the Metallurgical Society of AIME, 245, 1897–1902.

Ness, N.F., Behannon, K.W., Lepping, R.P., and Whang, Y.C. (1975) The magnetic field of Mercury, 1. Journal of Geophysical Research, 80, 2708–2716.

Nishida, K., Terasaki, H., Ohtani, E., and Suzuki, A. (2008) The effect of sulfur content on density of the liquid Fe-S at high pressure. Physics and Chemistry of Minerals, 35, 417–423.

Pavese, A. (2002) Pressure-volume-temperature equations of state: a comparative study based on numerical simulations. Physics and Chemistry of Minerals, 29, 43–51.

Ryzhenko, B. and Kennedy, G.C. (1973) The effect of pressure on the eutectic in the system Fe–FeS. American Journal of Science, 273, 803–810.

Sakamaki, T., Ohtani, E., Urakawa, S., Suzuki, A., and Katayama, Y. (2009) Measurement of hydrous peridotite magma density at high pressure using X-ray absorption method. Earth and Planetary Science Letters, 287, 293–297.

——— (2010) Density of dry peridotite magma at high pressure using an X-ray absorption method. American Mineralogist, 95, 144–147.

Sanloup, C., Guyot, F., Gillet, P., Fiquet, G., Mezouar, M., and Martinez, I. (2000) Density measurements of liquid Fe-S alloys at high-pressures. Geophysical Research Letters, 27, 811–814.

Sarson, G.R., Jones, C.A., Zhang, K., and Schubert, G. (1997) Magnetoconvection dynamos and the magnetic fields of Io and Ganymede. Science, 276, 1106–1108.

Schubert, G., Zhang, K., Kivelson, M.G., and Anderson, J.D. (1996) The magnetic field and internal structure of Ganymede. Nature, 384, 544–545.

Selivanov, E.N., Vershinin, A.D., and Gulyaeva, R.I. (2003) Thermal expansion of troilite and pyrrhotine in helium and air. Inorganic materials, 39, 1097–1102.

Seltzer, S.M. (1993) Calculation of photon mass energy-transfer and mass energy-absorption coefficients, Radiation Research, 136, 147–170.

Sharp, W.E. (1969) Melting curves of sphalerite, galena, and pyrrhotite and the decomposition curve of pyrite between 30 and 65 kilobars. Journal of Geophysical Research, 74, 1645–1652.

Solomon, S.C., Aharonson, O., Aurnou, J.M., Banerdt, W.B., Carr, M.H., Dombard, A.J., Frey, H.V., Golombek, M.P., Hauck, S.A. II, Head, J.W. III, and others. (2005) New perspectives on ancient Mars. Science, 307, 1214–1220.

Stevenson, D.J. (1987) Mercury's magnetic field: A thermoelectric dynamo? Earth and Planetary Science Letters, 82, 114–120.

Tenailleau, C., Etschmann, B., Wang, H., Pring, A., Grguric, B.A., and Studer, A. (2005) Thermal expansion of troilite and pyrrhotite determined by in situ cooling (873 to 373 K) neutron powder diffraction measurements. Mineralogical Magazine, 69, 205–216.

Urakawa, S., Morishima, M., Kato, T., Suzuki, A., and Shimomura, O. (1993) Equation of state for h-BN. Photon Factory Activity Report G, 275, 383.

Urakawa, S., Igawa, N., Kusaba, K., Ohno, H., and Shimomura, O. (1998) Structure of molten iron sulfide under high pressure. Review of High Pressure Science and Technology, 7, 286–288.

Urakawa, S., Someya, K., Terasaki, H., Katsura, T., Yokoshi, S., Funakoshi, K., Utsumi, W., Katayama, Y., Sueda, Y., and Irifune, T. (2004) Phase relationships and equations of state for FeS at high pressures and temperatures and implications for the internal structure of Mars. Physics of the Earth and Planetary Interiors, 143–144, 469–479.

Vinet, P., Rose, J.H., Ferrante, J., and Smith, J.R. (1989) Universal features of the equation of state of solids. Journal of Physics: Condensed Matter, 1, 1941–1963.

Manuscript received May 31, 2010
Manuscript accepted December 14, 2010
Manuscript handled by Guoyin Shen